Sensors and Actuators B 221 (2015) 1321–1329

Contents lists available at ScienceDirect

Sensors and Actuators B: Chemical

journal homepage: www.elsevier.com/locate/snb

Mixed-potential-type YSZ-based sensor with nano-structured NiO and porous TPB processed with pore-formers using coating technique

Xiaoyang Cheng [a], Chen Wang [a], Biao Wang [b], Ruize Sun [a], Yingzhou Guan [a], Yanfeng Sun [a,*,1], Xishuang Liang [a], Peng Sun [a], Geyu Lu [a,*]

[a] State Key Laboratory on Integrated Optoelectronics, College of Electronic Science and Engineering, Jilin University, 2699 Qianjin Street, Changchun 130012, China

[b] State Key Laboratory of Luminescence and Application, Changchun Institute of Optics, Fine Mechanics and Physics, Chinese Academy of Sciences, Changchun 130033, China

ARTICLE INFO

Article history:
Received 27 April 2015
Received in revised form 29 June 2015
Accepted 25 July 2015
Available online 29 July 2015

Keywords:
Mixed-potential-type NO_2 sensor
YSZ
TPB
Coating
Tape-casting
Pore-formers

ABSTRACT

In order to fabricate a high performance triple-phase-boundary (TPB) for a mixed potential type NO_x sensor based on stabilized zirconia and oxide electrode, a porous surface of the yttria-stabilized-zirconia substrate (YSZ) was formed with pore-formers (PMMA, graphite and starch) using coating technique. SEM observation result indicated that the porous morphology in the final ceramic was related to the category and amount of the pore formers, so that the pore size and microstructure of YSZ layer could be controlled. The NO_2 gas sensors using above-mentioned modified YSZ substrate with porous surface and nano-structured NiO electrode were fabricated and evaluated. The electric potential difference (ΔV) of the sensors varied almost linearly with the logarithm of NO_2 concentrations in the examined range of 10–500 ppm at 800 °C. The sensor based on 10 wt% starch-added YSZ matrix showed the largest response with the ΔV of 114 mV to 100 ppm NO_2. It was also seen that the sensors showed good response-recovery transient, selectivity and repeatability to NO_2.

1. Introduction

With the rapid increasing of the exhaust emissions from the automotive vehicles and various industrial processes, the content of nitrogen oxides (NO_x) have grown speedily in the air and give rise to severe environmental pollution such as acid rain and photochemical smog [1–8]. In order to effectively monitor the NO_x from car exhaust, the high performance NO_x sensor which is used in the on-board diagnostics (OBD) system for vehicles has been urgently demanded [1–6]. However, the NO_x sensor used for monitoring the vehicle exhaust must be operated under high temperature, high humidity and many coexisting gases, so the materials used for the NO_x sensor are required to have excellent chemical and thermal stability, and relatively low fabrication cost as well. All in all, various solid-electrolyte-based electrochemical NO_x sensing devices have been studied and reported in the past years [7–20]. Among all of them, the mixed potential type NO_x sensors combining stabilized zirconia with the metal oxides show the practical potential under the severe atmosphere [21–27], and have been widely investigated.

In order to improve the sensing property of mixed potential type NO_x sensor, many attentions have been focused on searching for the sensing electrode materials and preparing the high performance triple-phase-boundary (TPB) by various techniques. For example, Miura et al. reported that the sensors using NiO, Cr_2O_3-WO_3 and $MnCr_2O_4$ could give excellent sensing properties to NO_2 at elevated temperature [13–22]. Lu et al. has fabricated rough surfaces of YSZ substrate with some special treatment techniques, such as HF corroding, the double-tape casting and laser fabrication methods [9–14]. On one hand, the composition of the sensing electrode materials plays an important role on the sensing property of the mixed potential type NO_x sensor based on YSZ. The oxide sensing electrodes such as NiO have been testified to have high electrochemical catalytic activity to NO_x [12–20,28]. On the other hand, the TPB is the reaction field where the electrochemical reactions take place. A large area of TPB can enlarge the contact area between YSZ and the sensing electrode, and supply more electrochemical activity sites. Therefore, the constructing strategy of TPB has been investigated by some researchers [11–14]. Among the various methods to fabricate TPB, increasing the surface porosity of YSZ substrate is an important candidate due to its simplicity and

* Corresponding author. Tel.: +86 431 85167808; fax: +86 431 85167808.
E-mail addresses: syf@jlu.edu.cn (Y. Sun), lugy@jlu.edu.cn (G. Lu).
[1] Tel: +86 431 85168384; fax: +86 431 85167808.

http://dx.doi.org/10.1016/j.snb.2015.07.104
0925-4005/

good reproducibility. Furthermore, there are a number of ways to synthesize porous ceramics. Template technique appears to be one of the simplest and most flexible methods to prepare the porous surface of YSZ [29–31].

In this work, we suggested the coating method to form a porous surface of YSZ ceramic which could provide a larger contacting interface between the YSZ plate and the sensing electrode. High performance mixed-potential type NO_x sensor using the as-processed YSZ substrate and nano-structured NiO sensing electrode was fabricated and evaluated. Compared to the sensor without porous YSZ substrate, the sensing device using the porous YSZ substrate exhibited much higher response to NO_2.

2. Experimental

2.1. Preparation of YSZ layer by tape-casting method

The dense YSZ substrates were fabricated by YSZ powder (ZrO_2, 8 mol% Y_2O_3, KCM Corp., Japan) using tape-casting method [32,33]. The ceramic slurry was prepared by ball-milling YSZ power, triethanolamine (Aladdin Corp., China), polyvinyl butyral (PVB, Aladdin Corp., China), diethyl phthalate (DEP, Beijing Chemical Works, China), ethanol and butanone for 24 h. The resulted slurry were firstly vacuum bubbled for 1 h, and then fabricated as the basal tape with a thickness of 3 mm using the tape-casting equipment (Beijing Orient Sun-technical Corp., China). After drying the tape at 25 °C for 48 h and keeping it at 60 °C for another 73 h, a biscuit was achieved. The as-prepared biscuit was sintered at 1500 °C for 3 h in the air and then followed by cutting (2 cm × 2 cm). Consequently, the thickness of resulted YSZ substrate was reduced to 0.3 mm.

2.2. Fabrication and characteristics of the highly porous triple-phase interphase using coating method

In order to get the porous YSZ substrate, we modified the surface of YSZ-substrate with pore formers by coating method [29–31]. The schematic process of coating method is shown in Fig. 1. In this process, we prepared the coating ceramic slurry containing different pore formers (starch, graphite and polymethyl methacrylate) with varied doping ratio (5 wt%, 10 wt% and 15 wt%). The doping amounts, sizes and shapes of each pore formers are shown in Table 1.

Firstly, 50 mg (100 mg, 150 mg) of starch powders were dispersed in 1 g of above mentioned ceramic slurry under constantly ball-milling to prepare three kinds of coating slurries with different doping ratios of 5 wt%, 10 wt% and 15 wt%, respectively. Besides, in order to make a contrast between different pore formers, polymethyl methacrylate (PMMA) and graphite were also added to the above mentioned ceramic slurry with the mass ratio of 10 wt%, respectively. The as-prepared YSZ layer (2 cm × 2 cm) was masked perfectly into the mould (with inner length and width of 2 cm × 2 cm, and height of 0.5 mm) and left a groove on the surface. Coating slurry was dropped into the groove with 5 points once a time, and scratching the slurry along with the surface using a scraper immediately. After drying this slurry at 60 °C for half hour and repeating this procedure for another 3 times, followed by sintering at 1500 °C for 3 h, the integrated YSZ biscuit with porous surface was finally achieved.

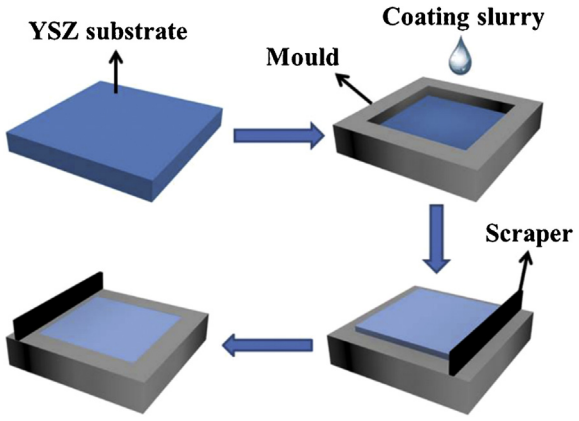

Fig. 1. Forming process schematic view of coating method.

Table 1
Characteristics of pore formers used in this investigation.

Ingredient	Amount of pore former (wt%)	Average particle size (um)	Particle shape
Starch	5% 10% 15%	50	Ellipsoid
PMMA	10%	80	Ball
Graphite	10%	40	Lamina

The composition and crystalline phase of the processed YSZ were investigated using X-ray diffraction on a Rigaku TTRIII X-ray diffractometer (using Cu Kα radiation at a wavelength of 1.5406 Å), and the data was collected from 20° to 80°. Thermogravimetric analysis and differential scanning calorimeter analysis (TG-DSC, Netzsch, STA449 F3 jupiter) were performed in air from 30 to 1300 °C at a heating rate of 10 °C/min to testify the thermal behaviors of the obtained slurries. The morphologies of final products were observed by field-emission scanning electron microscopy (SEM) on a JSM-7500F (JEOL) microscope operating at 15 kV.

2.3. Preparation and characterization of the nano-structured NiO

The nano-structured nickel oxide was prepared by a hydrothermal method [34–36]. In the typical synthesis process, 2.4 g of $NiCl{\cdot}6H_2O$, 0.6 g CTAB (cetyl trimethyl ammonium bromide) and 1.2 g of HMAT (Hexamethyleneteramine) were dissolved into a mixed solution containing 15 ml of deionized water and 15 ml of ethanol to form a clear solution. The solution was then transferred into a 40 ml Teflon-lined stainless-steel autoclave and kept at 160 °C for 12 h. After the autoclave cooling down to room temperature, the precipitate was centrifuged and washed with deionized water and ethanol for several times, and then dried at 80 °C for 24 h. Finally, the nano-structured NiO was obtained by sintering the precipitate at 1100 °C for 3 h in air.

2.4. Fabrication and evaluation of sensor

The mixed-potential-type NO_2 sensor was fabricated using the as-prepared porous YSZ-substrate and as-synthesized NiO. The detailed structure is shown in Fig. 2. On one end of YSZ-substrate, a narrow stripe-shaped Pt acting as reference electrode was coated with the commercial Pt paste (Sino-platinum Metals Co., Ltd.), and a Pt lead wire was attached on this Pt electrode. On the other end, a spot-shaped Pt paste was utilized for fixing another Pt lead wire, and then the as-synthesized NiO layer was formed on the spot-shaped Pt as the sensing electrode. The resulted sensing device was sintered at 1000 °C for 2 h. Then, a Pt heater formed on Al_2O_3 substrate was attached to the device by inorganic adhesive. According to the categories and doped ratio of pore formers, the sensors were labeled as S0 (the smooth substrate without doping any pore formers), S5 (5 wt% starch-added matrix), S10 (10 wt% starch-added matrix), S15 (15 wt% starch-added matrix),

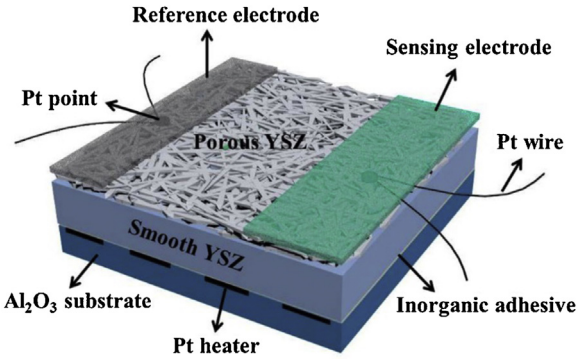

Fig. 2. Schematic view of the sensor structure.

P10 (10 wt% PMMA-added matrix) and G10 (10 wt% graphite-added matrix), respectively.

In order to check whether the NiO sensing electrode could combine with the porous surface of YSZ very well after sintering, we observed the cross section of the TPB by FESEM. Besides, to further testify the conjunction, we polished the NiO layer away on the porous YSZ plate and took the energy dispersive X-ray spectrometry (EDX) measurement by the SEM attachment to find out if the nano-particles had successfully dipped into the as-prepared pore structure.

The measurements of gas sensing characteristics were performed using a conventional static mounting method. The Pt heater kept the working temperature of the sensor at 800 °C. The various concentrations of NO_2 ranging from 10 to 500 ppm were prepared by diluting a parent gas (NO_2 balanced by 21 vol.% O_2 and 79 vol.% N_2) with air. The potential difference measured between air and sample gas (ΔV) was recorded as the sensing signal by a measurement unit (Digital Multimeter; Rigol Technologies, Inc., DM3054, China)

3. Results and discussion

3.1. Characterization of porous YSZ plate

Fig. 3 displays the XRD patterns of YSZ substrate sintered at 1500 °C. From which, the as-prepared product was identified as the single phase $Y_{0.15}Zr_{0.85}O_{1.98}$ (JCPDS file No. 30-1468) with a suitably crystalline hexagonal structure. No peaks from other phases were found, which suggested high purity of the as-synthesized YSZ.

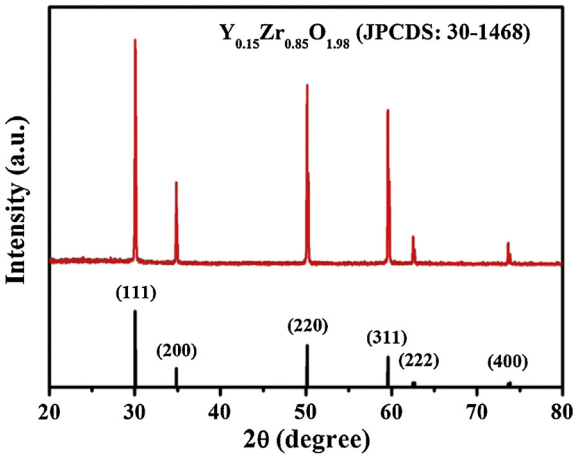

Fig. 3. The XRD patterns of YSZ ceramic substrate sintered at 1500 °C.

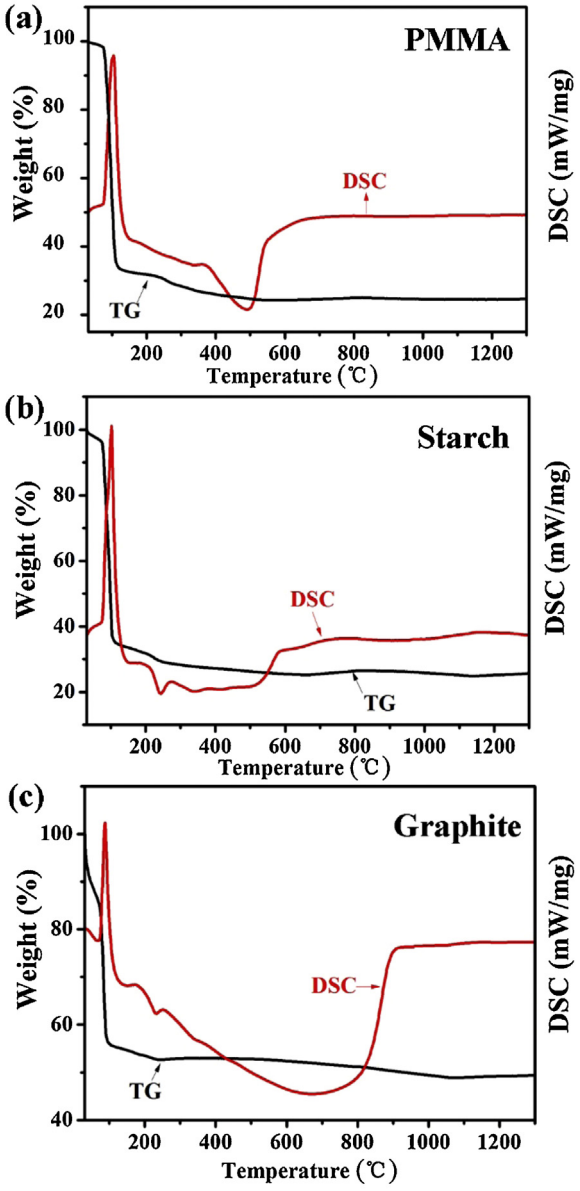

Fig. 4. The TG-DSC curves of the as-synthesized coating ceramic slurry with 10 wt% (a) PMMA; (b) starch; (c) graphite.

Fig. 4 shows the TG-DSC curves of the as-prepared coating ceramic slurry with 10 wt% PMMA, starch and graphite, respectively. As shown in Fig. 4, during the calcinations process, the organic species were released and decomposed from the matrix along with the phase formation process at corresponding crystallization temperatures. The endothermic peak at about 90–100 °C in three graphs could mainly be attributed to desorption or release of solvent included in the slurry, such as physically adsorbed water, ethanol, butanone, etc. Three main weight loss processes within different temperature range can be observed in Fig. 4a–c separately. First, in the range of 200–500 °C (Fig. 4a) slight weight loss appeared and accompanied with endothermic behavior, which demonstrated slow degradation of PMMA composition. Similarly, the mainly weight loss on TG curve and endothermic peaks on DSC curve shown in Fig. 4b and c indicated that starch was completely removed at 700 °C and graphite was burned out at 1000 °C. Within these temperature ranges, some tiny exothermic steps which could be attributed to the gradual crystallization of YSZ could also be seen. However, the crystal size continued to grow up after pore

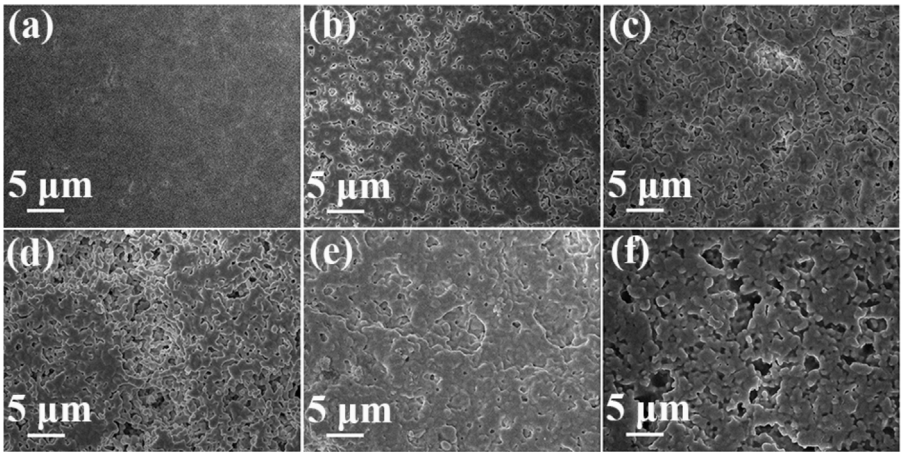

Fig. 5. Sintered porous YSZ ceramic microstructures made by adding pore formers: (a) smooth ceramic; (b) 5 wt% starch; (c) 10 wt% starch; (d) 15 wt% starch; (e) 10 wt% PMMA; (f) 10 wt% graphite.

formers evaporating, and the internal porosity would reduce as the YSZ particles growing. According to the above information, we can conclude that pore size made by PMMA would be smallest, and the biggest would be contributed by graphite.

Different pore formers can construct different morphology of substrate. As shown in Fig. 5, morphologies of the as-prepared YSZ using different pore formers are clearly indicated by SEM images. Fig. 5a shows the surface of YSZ without doping any pore formers which was certified to be smoothly. The sintered microstructures of porous ceramic with 5 wt%, 10 wt%, and 15 wt% starch-added matrixes are illustrated in Fig. 5b–d respectively. The porous structures obviously demonstrated that adding pore formers to the casting slurry can develop the porosity in the subsequently sintered process. The formation of such pore structure could be attributed to the evaporation of pore formers from the YSZ matrix when sintered at a high temperature of 1500 °C. These figures indicate that the size of pore was increased with raising the starch content. However, excessively porous interspace collapsed a lot in the 15 wt% starch-added matrix because of the instability. Close examination of Fig. 5c, e and f reveals several phenomena, which indicate that morphology of pores was closely connected with the characters of pore formers. It clearly verifies what have been concluded above that the pores made by PMMA were small, spheroidal and with well dispersibility. What's more, graphite constructed the unordered and biggest pores accompanied with collapse. By comparison, it showed increased porosity throughout the starch-added matrix than the PMMA-added matrix. Besides, starch-added matrix showed well-distributed pore microstructure and appropriate pore size, effectively avoided the collapse phenomenon similarly in the graphite-added matrix.

As followed, the characterization is further investigated by the SEM pattern of cross section of sintered ceramic substrate (Fig. 6a–c). Fig. 6d–f illustrates the schematic diagram of Fig. 6a–c respectively. It shows that similar thicknesses could be observed in all samples, and the average thickness of the porous YSZ layer was about 30 μm. As shown in Fig. 6a and d, 10 wt% PMMA-added matrix constructed evenly dispersed spheroidal microstructure pores within the substrate. When it came to 10 wt% starch-added matrix (Fig. 6b and e), there appears to be increasingly connected open pore structure with vertical distribution throughout the matrix as a result of the totally evaporation of starch particles. As a contrast, 10 wt% graphite-added matrix (Fig. 6c and f) showed horizontally porous banding structure. However, it could not benefit the nano-sized sensing particle accessing into the electrolyte as well as the vertical linked access (in Fig. 6b) could do. As a consequence, the porous microstructure and total porosity can be effectively controlled by the amount and category of the pore formers. What's more, these figures indicated that the overall trend respect to the various pore formers was in agreement with as-forecasted rules in TG-DSC curves. It can be even speculated that the

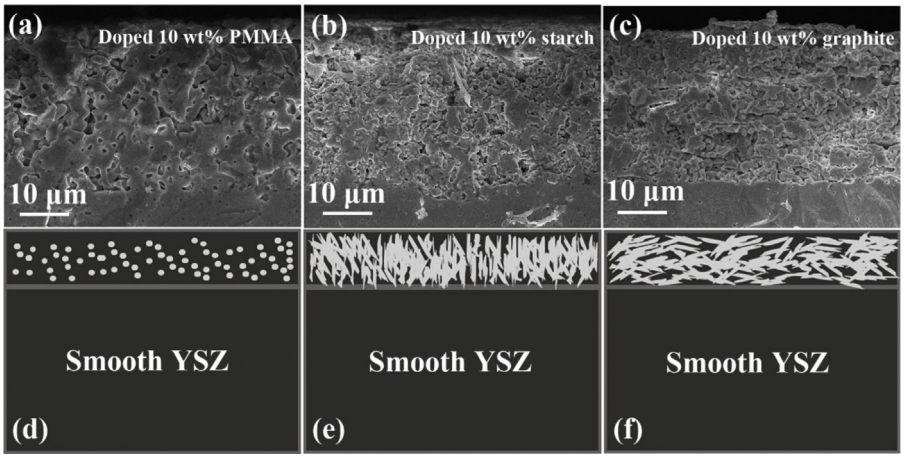

Fig. 6. The SEM pattern of cross section microstructures added various pore formers: (a) 10 wt% PMMA; (b) 10 wt% starch; (c) 10 wt% graphite; (d) schematic diagram of a; (d) schematic diagram of b; (d) schematic diagram of c.

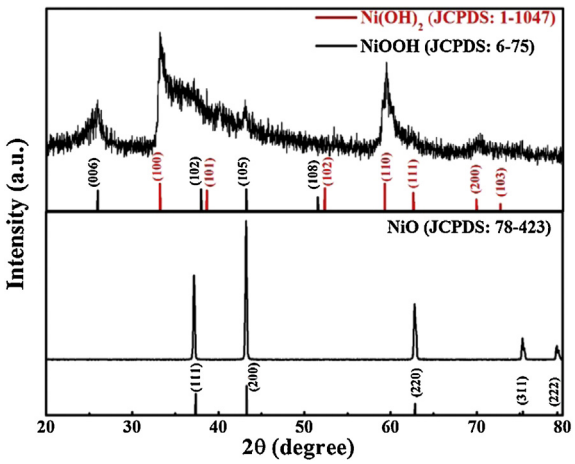

Fig. 7. The XRD patterns of (a) as-synthesized NiO precursor; (b) the nano-structured NiO sintered at 1100 °C.

10 wt% starch-added matrix will result into the most appropriate modification of porous YSZ substrate and be the main contributing factor for improving NO_2 sensitivity of the sensor.

3.2. Crystal-phase composition and morphology of nano-structured NiO sensing electrodes

The powder X-ray diffraction pattern of as-synthesized precursor is shown in Fig. 7a. The precursor showed a mixture of seven typical diffraction peaks which could be indexed to hexagonal structured $Ni(OH)_2$ (JCPDS card No. 1-1047) and four other peaks indexed to hexagonal structured NiOOH (JCPDS card No. 6-75). As shown in Fig. 7b, the resulted NiO was identified as single phase NiO with suitably crystalline cubic structure (JCPDS file No. 78-432), which revealed that the nano-structure nickel oxide were obtained after calcination of $Ni(OH)_2$ and NiOOH at 1100 °C for 3 h.

The SEM images of Fig. 8a demonstrates the detailed structure of the as-prepared precursor, from which a flowerlike morphology with an average size of 4 um was clearly observed. As shown in Fig. 8b, the morphology of assembled NiO maintained a basic sphere shape of the precursor. From the higher magnification SEM image shown in the inset, we can see that the assembled NiO particles were composed by many nano-cubic-particles. Obviously, NiO grew in an oriented manner to form an integrated porous architecture. According to these, we can conclude that during the sintering process, the flowerlike surface of the 3D structure in precursor was collapsed step by step. This process effectively slowed down the growth of basic NiO particle and formed the smaller size. As the temperature getting higher, the NiO particle began to grow up slowly. After sintering in 1100 °C for 3 h, the resulted particle eventually grew up with well dispersibility (shown in the inset of Fig. 8b).

3.3. The characterization of TPB covered with nano-structured NiO

Fig. 9 shows the morphologies of TPB prepared by 10 wt% starch-added matrix and nano-structured NiO powders. On one hand, Fig. 9a displays the SEM pattern of cross section part of the TPB, where NiO sensing electrode film deposited onto the as-fabricated porous YSZ substrate. The interface between the NiO film and the YSZ substrate can be clearly seen in this figure. The high-magnification SEM micrograph clearly indicates that the NiO nano-particles were perfectly filled into the as-prepared pores and constructed a high quality TPB with larger effective contacting area. As the TPB is the field in which the target gases take electrochemical reactions, the high quality TPB can supply more active sites for the related electrochemical reactions and obviously improve the sensing characteristics.

On the other hand, Fig. 9b–e is the scanning EDX image of polished porous ceramic plane. EDX elemental mapping was conducted to clearly confirm the spatial distribution of Ni and YSZ (Y_2O_3–ZrO_2) in the composite structure. The EDX analysis shows the Ni (Fig. 9c), Y (Fig. 9d) and Zr (Fig. 9e) contents, respectively. After detailed observation and combined analysis, the places circled out were testified as the as-prepared pores because the signals of Y and Zr detected in the corresponding locations were pretty weak. Oppositely, the Ni signals there densely covered this dark region. Besides, we can see the signals of Ni were detected to be regularly dispersed and clearly agglomerated over the substrate, which also indicated that the nano-structured NiO particles were uniformly distributed and perfectly dipped into the as-prepared pore structures of TPB.

The TPB of original dense substrate is marked as the red line in Fig. 10a. As we discussed, the interface of the YSZ with pore former added matrix became porous after being sintered. The porous structure can realize the deposition of nano-structured NiO sensing particles into the connected pore structure, and then provide larger contact area between electrolyte and sensing electrode material to elongate the TPB length, which is also marked using the red line as schematically depicted in Fig. 10b. Under this circumstance, the increased TPB length can supply more active sites for the related electrochemical reactions and accelerate reactions. Make the comparison between the two red lines in Fig. 10, we can see that the length of the TPB can be effectively increased by enhancing the porosity. In other words, the NO_2 sensitivity can be significantly enhanced by improving the porosity of TPB. Specifically, 10 wt% starch-added matrix with vertical distributed pore structure should be much more effectively than others to fulfil the deeper infiltration of NiO and longer length of TPB, which indicates the sensor

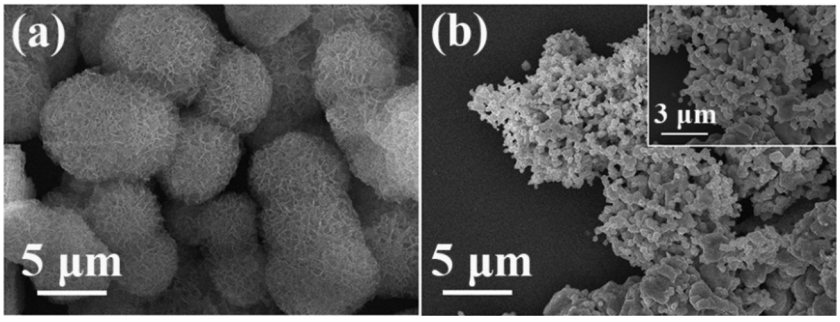

Fig. 8. The SEM patterns of (a) as-synthesized NiO precursor and (b) sensing oxides NiO calcined at 1100 °C.

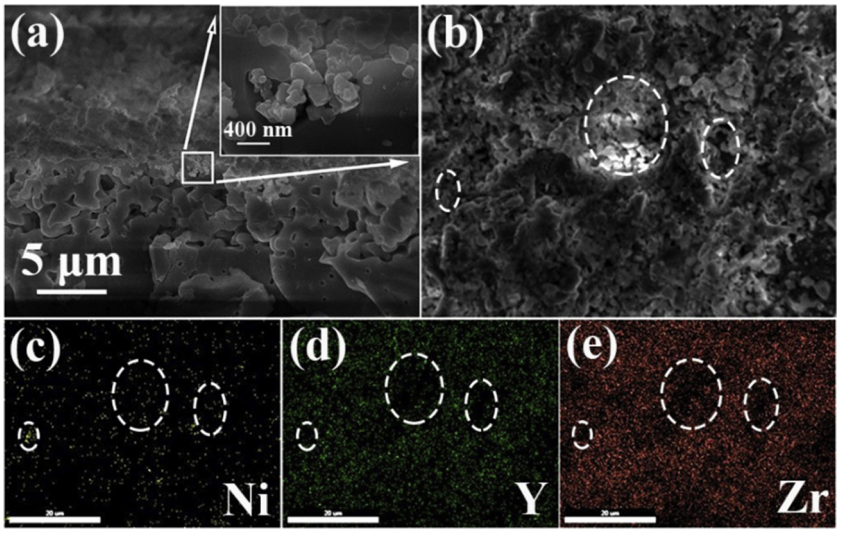

Fig. 9. Representative SEM images of (a) the cross sectional view and (b) top view of porous TPB (doping 10 wt% starch) attached with the NiO-SE sintered at 1000 °C. EDS observation for the element of (c) Ni, (d) Y, and (f) Zr.

attached with 10 wt% starch-added matrix should show the highest sensitivity.

3.4. Sensing performances of the NO_2 sensors

In order to better illustrate the connection between porous YSZ substrate and the sensing properties, the sensing mechanism is firstly introduced here. The sensing characteristic of this kind of potentiometric sensor agrees with the mixed potential mechanism which has been verified by Miura and co-workers [9,12,14,15]. According to that, the sensor can be described as the following electrochemical cells:

In air: O_2, NiO/YSZ/Pt, O_2

In target gas: $O_2 + NO_2$, NiO/YSZ/Pt, $NO_2 + O_2$

In air, only the following equilibrium takes place at each electrode:

$$1/2O_{2(gas)} + V_O^{\bullet\bullet} + 2e^- \rightarrow O^{2-}(YSZ) \quad (1)$$

Here, $V_O^{\bullet\bullet}$ represents the oxygen vacancy in the YSZ. Electronic charge transfers between Pt electrodes and the zirconia electrolyte as oxygen is incorporated or removed from the zirconia lattice. Apparently, the transmission speed of the O^{2-} here in the solid electrolyte can affect the total reaction rate.

Under the target gas atmosphere, two electrochemical reactions (2) and (3) simultaneously take place at the sensing electrode.

$$\text{Cathodic}: NO_2 + 2e^- \rightarrow NO + O^{2-}(YSZ) \quad (2)$$

$$\text{Anodic}: 2O^{2-}(YSZ) \rightarrow O_2 + 4e^- \quad (3)$$

The above electrochemistry reactions occur at the active sites of TPB. When the rates of reactions (2) and (3) are equal, a local cell forms and the potential in the sensing electrode is called the mixed potential. The electric potential difference between the sensing electrode and reference electrode is potential difference (ΔV).

Fig. 11a shows the continuous response and recovery transients to 10–500 ppm NO_2 for Sensor S0, S5, S10 and S15 at 800 °C. It is seen that all sensors responded well to NO_2 and the steady-state ΔV values attained at each NO_2 concentration were rather quick. And the increase or decrease in the sensing characteristic was substantiated by the results of the measurements. Firstly, the sensor S0 showed a high ΔV with 59 mV to 100 ppm NO_2 at 800 °C, which was larger than those had reported before by Liang and co-workers [9–16]. As for the reason, it should be that the smaller nano-particles of oxide can effectively promote the sensing characteristic, which was reported by Diao et al. [22]. Compared to S0, the ΔV of S10 to 100 ppm NO_2 was 114 mV at 800 °C, while the ΔV of sensor S5 and S15 were 68 mV and 83 mV, respectively. In other words, the ΔV values to NO_2 in the range of 10–500 ppm at 800 °C for improved sensors (S5, S10 and S15) had increased, which clearly showed that the increase of porosity can effectively enhance the sensitivity. Besides, it should be noted that the sensor based on 10 wt% starch-added matrix (S10) showed the highest potential difference. It meant that the sensitivity firstly got continual promotion as the doping ratio of the pore formers confined increased, but then conversely receded with the pore formers doping too much.

Under these circumstances, various factors are discussed to seek the reasons. What has previously reported is that the conductivity of the solid electrolyte declined when its porosity gets promoted. The details in this regard have been discussed sufficiently by

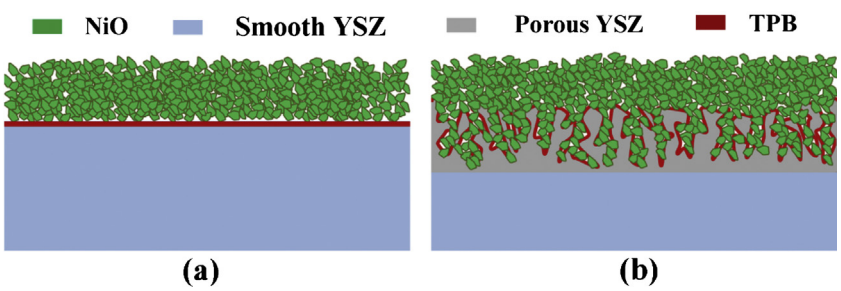

Fig. 10. Schematic view of (a) original TPB and (b) modified TPB.

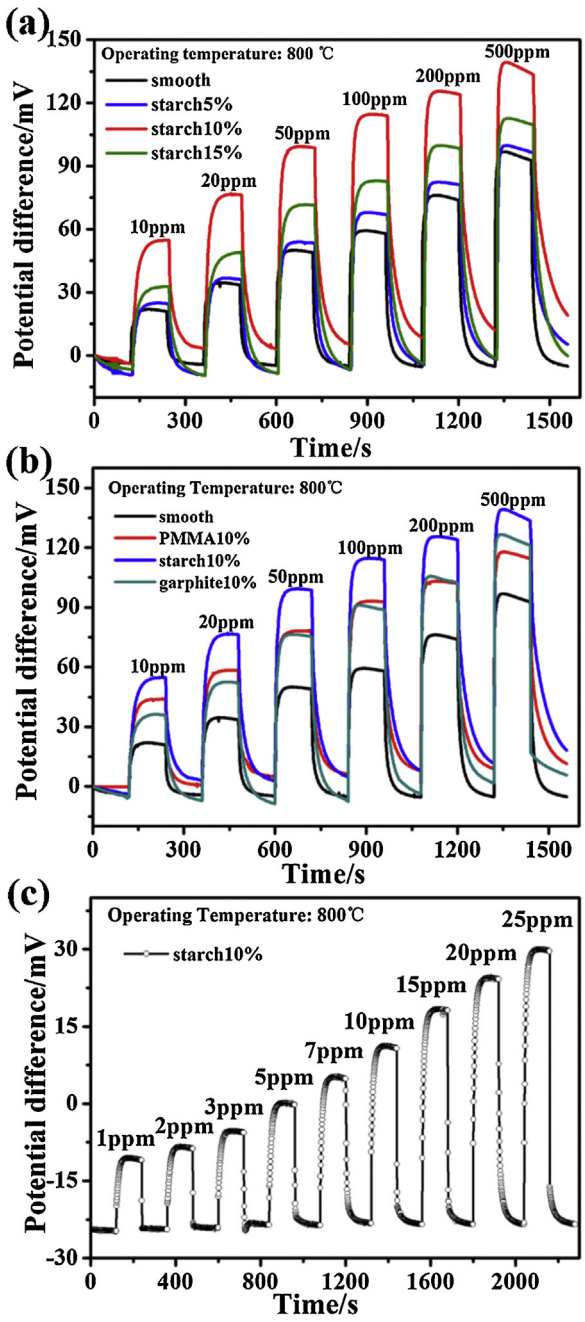

Fig. 11. Response transients of sensors (a) S0, S5, S10, and S15; (b) S0, S10, P 10, and G10 to 10–500 ppm NO_2 concentrations; (c) Response transients of sensor S10 to 1–25 ppm NO_2 at 800 °C.

Baumgartner et al. [37,38] and Suzuki et al. [39]. In view of the fact that the sensitivity kept increasing as the doping ratio increased from 5% to 10%, even the conductivity of YSZ reduced slightly, the main reason should be attributed to the better porosity can provide larger contact area of as-constructed TPB, supply more active sites for the related electrochemical reactions and then hugely accelerate the reactions to a great extent at same time. The latter reason must be accounted overwhelmed than the former reason. Conversely, as the doping ratio keeping arisen to 15%, such too porous substrate would be the main restriction reason to drastically reduce the conductivity, which would weaken and even retard the propagation speed of O^{2-} and then result into slower rate of exchange reaction between the adsorbed oxygen on the interface of TPB and the oxygen ions existing in the bulk of YSZ. What's worse, such excessive porosity with collapse (evident from Fig. 5d) would decrease the actual amount of reaction sites at the interface between 15 wt% starch-added YSZ and NiO sensing electrode. And hence, S15 is expected to show diminished NO_2 sensitivity compared to S10.

We further tested the sensing properties of sensors P10 and G10 to make a comparison with S10, aiming to find out a difference caused by different pore formers. Fig. 11b exhibits the response transients to NO_2 (10–500 ppm) for the sensor S0, P10, S10 and G10 at 800 °C. In which, all sample sensors all presented a large increase of the response to NO_2. As a result, S10 still showed the largest ΔV. This could be attributed to the connected open pore structure with vertical distribution constructed by starch which benefited the nano-sized NiO particles to infiltrate into the electrolyte to elongate the TPB length at the greatest extent.

Fig. 11c exhibits the measured results of response transients to 1–25 ppm NO_2 for S10. After further observation of the response transients, it turned out that all sample sensors improved by coating method showed well sensing characteristic and larger ΔV to low concentration of target gas than reported before. These sensors (S10, etc.) show potential advantage in detecting the low concentration of NO_2 which is meaningful to monitor the NO_x and control atmosphere pollution.

Thus, in all cases, the ΔV value changed quickly upon exposure to 100 ppm NO_2 at 800 °C and soon reached the steady-state value. The 90% response time for sensor S0 to 100 ppm NO_2 was 10 s, the 90% response time for modified sensors (S5, S10, S15, P10 and G10) was corresponding 12–14 s. Secondly, the recovery rate became much slower with the increasing porosity of the YSZ substrate. While the 90% recovery times of S0 was 20 s, the ΔV response of S5, S10, S15, P10 and G10 did not return to the original level after nearly 1 min with 63 s, 66 s, 68 s, 59 s and 60 s, respectively. Such a slow recovery rate seems to be caused by the low electrochemical reaction speed, which can be attributed to the porous structure at the interface of TPB. Because the pore structure can supply larger contact area and more active sites which can enhance the adsorption once response to NO_2 and improve the ΔV. However, porosity will also in return obstruct the desorption and diffusion process of target gas during the recovery process. It is seen in Fig. 11c that the 90% response times of the sensor S10 to 1 ppm and 25 ppm NO_2 are about 14 s and 16 s which were similar, but the 90% recovery times were 3 s and 8 s, respectively. It showed that as the concentration of NO_2 increased, the same device absorbed much more target gas to the electrochemical active sites at the same time, and in return caused the slower desorption which resulted into a lower recovery rate. As discussed above, Fig. 11a–c shows that each sensor had acceptable response and recovery time which could meet the basic needs of detecting task. However, recovery rate acted as important characteristics as well for a practical NO_2 sensor, still need more efforts to further examined and improved.

Dependence of the potential difference on the NO_2 concentrations for the sensor S10 using NiO is shown in Fig. 12. It is seen that the ΔV of the sensor varied linearly with the logarithm of NO_2 concentration in the examined range of 10–500 ppm at 800 °C. The slope of the S10 with 10 wt% starch-added matrix was about 60 mV/decade, while the S0 using smooth one was about 38 mV/decade. It was obvious that the slope became larger when the porosity increased, which indirectly indicated that the improvement of the effective area of TPB played an important role in increasing the sensitivity (slope) of the sensor.

The present sensor device S10 was further subjected to additional test for the cross-sensitivities test to various gases. As shown in Fig. 13, S10 exhibited high selectivity to 100 ppm NO_2 against the interference gases with the ΔV of more than 110 mV, and a rather low response to others with ΔV of less than 10 mV. These well sensing properties indicated promising potential advantage of

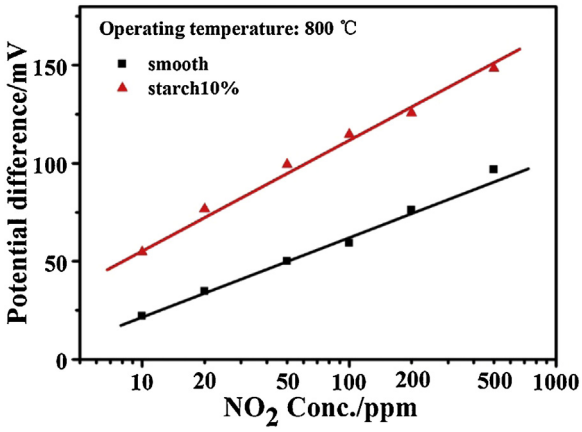

Fig. 12. Dependence of potential difference on the NO_2 concentration for the sensor S10 using the YSZ substrate doping 10 wt% starch.

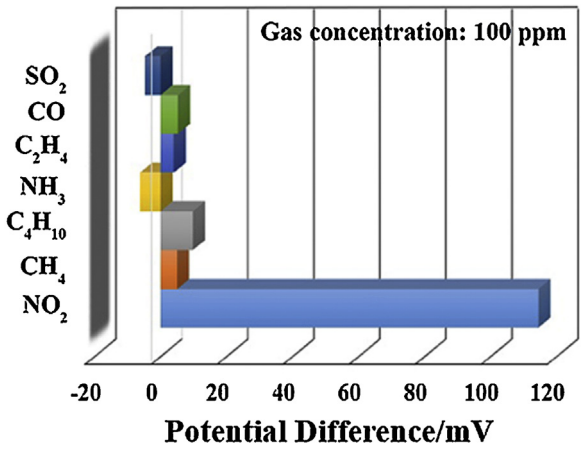

Fig. 13. Sensitivities of the sensor S10 using the YSZ substrate doping 10 wt% starch that to various gases at 800 °C.

the sensor in practical application. As shown in Fig. 14, the response transients as well as the potential difference response to 100 ppm NO_2 also showed reproducible properties in successive runs. This result confirms that the reproducibility of the improved device is really good.

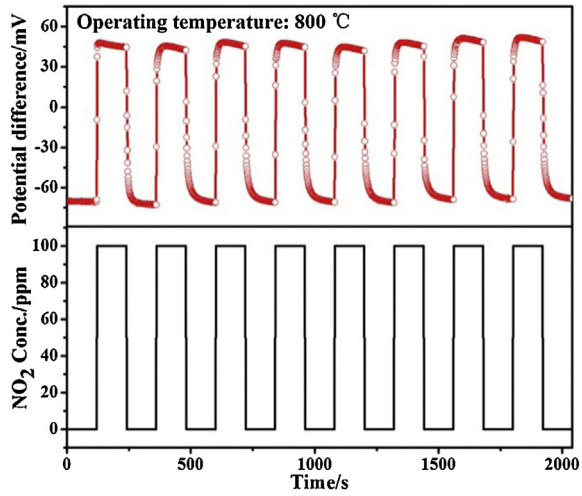

Fig. 14. Repeated response transients of the sensor S10 using the YSZ substrate doping 10 wt% starch upon switching on- and off-NO_2 repeatedly at 800 °C.

4. Conclusions

In summary, the porous and stable triple-phase-boundary (TPB) structure of YSZ substrate has been successfully prepared using coating techniques with various pore formers, and the nano-structured NiO was synthesized by hydrothermal method as the sensing electrode. The mixed-potential-type NO_2 sensor based on as-prepared porous TPB and NiO contributed to a remarkable increase of the response to NO_2 at the ranges from 10 ppm to 500 ppm, and the increased value showed a direct relationship to the category and amount of pore formers. Each sensor showed an acceptable response and recovery time to meet the basic needs of detecting task. The sensor based on the 10 wt% starch-added matrix showed the largest response to 100 ppm NO_2 with the ΔV of 114 mV at 800 °C. Further tests were taken and response varied linearly with logarithm of the concentration. Moreover, the sensor exhibited well selectivity and repeatability to NO_2. These well sensing properties indicate the promising potential of the sensor in practical application.

Acknowledgements

This work was supported by the National Nature Science Foundation of China (Nos. 61473132, 61374218, 61134010, and 61327804) and Program for Chang Jiang Scholars and Innovative Research Team in University (No. IRT13018). National High-Tech Research and Development Program of China (863 Program, No. 2013AA030902 and 2014AA06A505).

References

[1] P. Sekhar, E. Brosha, R. Mukundan, W. Li, M. Nelson, P. Palanisamy, F. Garzon, Application of commercial automotive sensor manufacturing methods for NO_x/NH_3 mixed potential sensors for on-board emissions control, Sens. Actuators B: Chem. 144 (2010) 112–119.
[2] F. Ménil, V. Coillard, C. Lucat, Critical review of nitrogen monoxide sensors for exhaust gases of lean burn engines, Sens. Actuators B: Chem. 67 (2000) 397–403.
[3] T. Ono, M. Hasei, A. Kunimoto, T. Yamamoto, A. Noda, Performance of the NO_x sensor based on mixed potential for automobiles in exhaust gases, JSAE Rev. 22 (2001) 49–55.
[4] S. Zhuiykov, N. Miura, Development of zirconia-based potentiometric NO_x sensors for automotive and energy industries in the early 21st century: what are the prospects for sensors? Sens. Actuators B: Chem. 121 (2007) 639–651.
[5] E.L. Brosha, R. Mukundan, D.R. Brown, F.H. Garzon, J.H. Visser, Development of ceramic mixed potential sensors for automotive applications, Solid State Ionics 148 (2002) 61–69.
[6] V. Plashnitsa, P. Elumalai, Y. Fujio, N. Miura, Zirconia-based electrochemical gas sensors using nano-structured sensing materials aiming at detection of automotive exhausts, Electrochim. Acta 54 (2009) 6099–6106.
[7] H.-C. Cho, S. Takase, J.-H. Song, Y. Shimizu, Sensing behavior of solid-state impedancemetric NO_x sensor using solid electrolyte transducer and oxide receptor, Sens. Actuators B: Chem. 187 (2013) 94–98.
[8] S. Fischer, R. Pohle, B. Farber, R. Proch, J. Kaniuk, M. Fleischer, R. Moos, Method for detection of NO_x in exhaust gases by pulsed discharge measurements using standard zirconia-based lambda sensors, Sens. Actuators B: Chem. 147 (2010) 780–785.
[9] G. Lu, Q. Diao, C. Yin, S. Yang, Y. Guan, X. Cheng, X. Liang, High performance mixed-potential type NO_x sensor based on stabilized zirconia and oxide electrode, Solid State Ionics 1 (2014) 292–297.
[10] Y. Guan, C. Li, X. Cheng, B. Wang, R. Sun, X. Liang, J. Zhao, H. Chen, G. Lu, Highly sensitive mixed-potential-type NO_2 sensor with YSZ processed using femtosecond laser direct writing technology, Sens. Actuators B: Chem. 198 (2014) 110–113.
[11] C. Yin, Y. Guan, Z. Zhu, X. Liang, B. Wang, Q. Diao, H. Zhang, J. Ma, F. Liu, Y. Sun, J. Zheng, G. Lu, Highly sensitive mixed-potential-type NO_2 sensor using porous double-layer YSZ substrate, Sens. Actuators B: Chem. 183 (2013) 474–477.
[12] X. Liang, S. Yang, J. Li, H. Zhang, Q. Diao, W. Zhao, G. Lu, Mixed-potential type zirconia-based NO_2 sensor with high-performance three-phase boundary, Sens. Actuators B: Chem. 158 (2011) 1–8.
[13] N. Miura, J. Wang, P. Elumalai, T. Ueda, D. Terada, M. Hasei, Improving NO_2 sensitivity by adding WO_3 during processing of NiO sensing-electrode of mixed-potential-type zirconia-based sensor, J. Electrochem. Soc. 8 (2007) 246–252.

[14] J. Park, B.Y. Yoon, C.O. Park, W.-J. Lee, C.B. Lee, Sensing behavior and mechanism of mixed potential NO_x sensors using NiO, NiO(+YSZ) and CuO oxide electrodes, Sens. Actuators B: Chem. 135 (2009) 516–523.
[15] N. Miura, J. Wang, M. Nakatou, P. Elumalai, S. Zhuiykov, M. Hasei, High-temperature operating characteristics of mixed-potential-type NO_2 sensor based on stabilized-zirconia tube and NiO sensing electrode, Sens. Actuators B: Chem. 114 (2006) 903–909.
[16] P. Elumalai, N. Miura, Performances of planar NO_2 sensor using stabilized zirconia and NiO sensing electrode at high temperature, Solid State Ionics 176 (2005) 2517–2522.
[17] T. Sato, V.V. Plashnitsa, M. Utiyama, N. Miura, Potentiometric YSZ-based sensor using NiO sensing electrode aiming at detection of volatile organic compounds (VOCs) in air environment, Electrochem. Commun. 12 (2010) 524–526.
[18] P. Elumalai, J. Zosel, U. Guth, N. Miura, NO_2 sensing properties of YSZ-based sensor using NiO and Cr-doped NiO sensing electrodes at high temperature, Ionics 15 (2009) 405–411.
[19] P. Elumalai, J. Wang, S. Zhuiykov, D. Terada, M. Hasei, N. Miura, Sensing characteristics of YSZ-based mixed-potential-type planar NO_x sensors using NiO sensing electrodes sintered at different temperatures, J. Electrochem. Soc. 7 (2005) 95–101.
[20] V. Plashnitsa, V. Gupta, N. Miura, Mechanochemical approach for fabrication of a nano-structured NiO-sensing electrode used in a zirconia-based NO_2 sensor, Electrochim. Acta 55 (2010) 6941–6945.
[21] Q. Diao, C. Yin, Y. Liu, J. Li, X. Gong, X. Liang, S. Yang, H. Chen, G. Lu, Mixed-potential-type NO_2 sensor using stabilized zirconia and Cr_2O_3-WO_3 nanocomposites, Sens. Actuators B: Chem. 180 (2013) 90–95.
[22] Q. Diao, C. Yin, Y. Guan, X. Liang, S. Wang, Y. Liu, Y. Hu, H. Chen, G. Lu, The effects of sintering temperature of $MnCr_2O_4$ nanocomposite on the NO_2 sensing property for YSZ-based potentiometric sensor, Sens. Actuators B: Chem. 177 (2013) 397–403.
[23] E.D. Bartolomeo, N. Kaabbuathong, M.L. Grilli, E. Traversa, Planar electrochemical sensors based on tape-cast YSZ layers and oxide electrodes, Solid State Ionics 171 (2004) 173–181.
[24] N.F. Szabo, P.K. Dutta, Correlation of sensing behavior of mixed potential sensors with chemical and electrochemical properties of electrodes, Solid State Ionics 171 (2004) 183–190.
[25] N. Miura, H. Jin, R. Wama, S. Nakakubo, P. Elumalai, V. Plashnitsa, Novel solid-state manganese oxide-based reference electrode for YSZ-based oxygen sensors, Sens. Actuators B: Chem. 152 (2011) 261–326.
[26] T. Striker, V. Ramaswamy, E.N. Armstrong, P.D. Willson, E.D. Wachsman, J.A. Ruud, Effect of nanocomposite Au–YSZ electrodes on potentiometric sensor response to NO_x and CO, Sens. Actuators B: Chem. 181 (2013) 312–318.
[27] Y. Guan, C. Yin, X. Cheng, X. Liang, Q. Diao, H. Zhang, G. Lu, Sub-ppm H_2S sensor based on YSZ and hollow balls $NiMn_2O_4$ sensing electrode, Sens. Actuators B: Chem. 193 (2014) 501–508.
[28] P. Elumalai, V.V. Plashnitsa, Y. Fujio, N. Miura, Highly sensitive and selective stabilized zirconia-based mixed-potential-type propene sensor using NiO/Au composite sensing-electrode, Sens. Actuators B: Chem. 144 (2010) 215–219.
[29] S.F. Corbin, J. Lee, X. Qiao, Influence of green formulation and pyrolyzable particulates on the porous microstructure and sintering characteristics of tape cast ceramics, J. Am. Ceram. Soc. 84 (2001) 41–47.
[30] F.C. Krebs, Fabrication and processing of polymer solar cells: a review of printing and coating techniques, Solar Energy Mater. Solar Cells 93 (2009) 394–412.
[31] F.C. Krebs, Polymer solar cell modules prepared using roll-to-roll methods: knife-over-edge coating, slot-die coating and screen printing, Solar Energy Mater. Solar Cells 93 (2009) 465–475.
[32] M. Boaro, J.M. Vohs, R.J. Gorte, Synthesis of highly porous yttria-stabilized zirconia by tape-casting methods, J. Am. Ceram. Soc. 86 (2003) 395–400.
[33] H. Kim, C.D. Rosa, M. Boaro, J.M. Vohs, R.J. Gorte, Fabrication of highly porous yttria-stabilized zirconia by acid leaching nickel from a nickel-yttria-stabilized zirconia cermet, J. Am. Ceram. Soc. 85 (2002) 1473–1476.
[34] Y. Wang, Q. Zhu, H. Zhang, Fabrication of β-$Ni(OH)_2$ and NiO hollow spheres by a facile template-free process, Chem. Commun. 41 (2005) 5231–5233.
[35] Y. Yang, R. Jin, S. Song, Y. Xing, Synthesis of flower-like nickel oxide/nickel silicate nanocomposites and their enhanced electrochemical performance as anode materials for lithium batteries, Mater. Lett. 93 (2013) 5–8.
[36] Q. Li, Y. Chen, T. Yang, D. Lei, G. Zhang, L. Mei, L. Chen, Q. Li, T. Wang, Preparation of 3D flower-like NiO hierarchical architectures and their electrochemical properties in lithium-ion batteries, Electrochim. Acta 90 (2013) 80–89.
[37] C.E. Baumgartner, R.H. Arendt, C.D. Iacovangelo, B.R. Karas, Molten carbonate fuel cell cathode materials study, J. Electrochem. Soc. 131 (1984) 2217–2221.
[38] M.A. van den Noort, P.J.J.M. van der Put, J. Schoonman, Doped $LiFeO_2$ as MCFC cathode material, High Temp.-High Pressures 20 (1988) 197–200.
[39] T. Suzuki, Z. Hasan, Y. Funahashi, T. Yamaguchi, Y. Fujishiro, M. Awano, Impact of anode microstructure on solid oxide fuel cells, Science 325 (2009) 852–855.

Biographies

Xiaoyang Cheng received the B.E. degree in Department of Electronic Science and Technology in 2013. She is currently studying for her M.S. degree in College of Electronic Science and Engineering, Jilin University, China.

Chen Wang received the B.E. degree in Department of Electronic Sciences and Technology in 2013. He is currently working toward the M.S. degree in the Electronics Science and Engineering Department, Jilin University. His research interests include the synthesis of functional materials and their applications in gas sensors.

Biao Wang obtained his Ph.D. degree from Jilin University, China in 2008. Now he is an Associate Research Professor in Changchun Institute of Optics, Fine Mechanics and Physics, Chinese Academy of Science. His current research is laser gas sensor.

Ruize Sun received the B.E. degree in Department of Electronic Science and Technology in 2012. He is currently studying for his M.S. degree in College of Electronic Science and Engineering, Jilin University, China.

Yingzhou Guan received the B.E. degree in Department of Electronic Sciences and Technology in 2012. He is currently studying for his M.S. degree in College of Electronic Science and Engineering, Jilin University, China.

Yafeng Sun obtained his Ph.D. from Jilin University of China in 2007. Presently, he is working as Associate Professor in Electronics Science and Engineering Department of Jilin University. His current research interests are nanoscience and gas sensors.

Xishuang Liang received the B.E. degree in Department of Electronic Science and Technology in 2004. He received his Doctor's degree from College of Electronic Science and Engineering at Jilin University in 2009. Now he is a lecturer of Jilin University, China. His current research is solid electrolyte gas sensor.

Peng Sun received his Ph.D. degree from the Electronics Science and Engineering Department, Jilin University, China in 2014. Now, he is engaged in the synthesis and characterization of the semiconducting functional materials and gas sensors.

Geyu Lu received the B.S. degree in electronic sciences in 1985 and the M.S. degree in 1988 from Jilin University in China and the Dr. Eng. degree in 1998 from Kyushu University in Japan. Now he is a Professor of Jilin University, China. Presently, he is interested in the development of functional materials and chemical sensors.